A Study on Blend Ratio-dependent Far-IR and Low-frequency Raman Spectra and WAXD Patterns of Poly(3-hydroxybutyrate)/poly(4-vinylphenol) Using Homospectral and Heterospectral Two-…

Marlina, Dian ; Park, Yeonju ; Hoshina, Hiromichi ; Ozaki, Yukihiro ; Jung, Young Mee ; Sato, Harumi

(Citation)
Analytical Sciences,36(6):731-737

(Issue Date)
2020-06-10

(Resource Type)
journal article

(Version)
Version of Record

ANALYTICAL SCIENCES JUNE 2020, VOL. 36

A Study on Blend Ratio-dependent Far-IR and Low-frequency Raman Spectra and WAXD Patterns of Poly(3-hydroxybutyrate)/poly(4-vinylphenol) Using Homospectral and Heterospectral Two-dimensional Correlation Spectroscopy

Dian MARLINA,*1,*2 Yeonju PARK,*3 Hiromichi HOSHINA,*4 Yukihiro OZAKI,*5,*6 Young Mee JUNG,*3† and Harumi SATO*1,*6†

*1 *Graduate School of Human Development and Environment, Kobe University, 3-11 Tsurukabuto, Nada, Kobe 657-8501, Japan*
*2 *Faculty of Pharmacy, Universitas Setia Budi, Surakarta, Central Java 57127, Indonesia*
*3 *Department of Chemistry, Institute for Molecular Science and Fusion Technology, Kangwon National University, Chuncheon 24341, Korea*
*4 *Center for Advance Photonic, RIKEN, Sendai, Miyagi 980-0845, Japan*
*5 *School of Science and Technology, Kwansei Gakuin University, Sanda 669-1337, Hyogo, Japan*
*6 *Molecular Photoscience Research Center, Kobe University, Nada, Kobe 657-8501, Japan*

An intensive analysis of far-infrared (far-IR), low-frequency Raman, and wide angle X-ray diffraction (WAXD) data has been performed by two-dimensional correlation spectroscopy (2D-COS) as a function of the blend ratio of poly(3-hydroxybutyrate)/poly(4-vinylphenol) (PHB/PVPh). Homospectral 2D-COS revealed that a weak band at 128 cm^{-1} in the far-IR spectra appeared more clearly in the 2D correlation spectra. Heterospectral 2D-COS (far-IR/low-frequency Raman and far-IR/WAXD) provided very important results that were hardly detected in the conventional 2D-COS. A far-IR peak at 130 cm^{-1} in the heterospectral 2D-COS had negative correlations with the peaks in the low-frequency Raman spectra at 81, 100, and 110 cm^{-1} and WAXD profile 8.78 and 11.01°. These results indicated that those peaks have different origins; the 130 cm^{-1} peak comes from the intermolecular C=O···H–O hydrogen bond between PHB and PVPh, while those for low-frequency Raman and WAXD peaks are the features of PHB crystalline structure.

Keywords PHB/PVPh, far-infrared spectroscopy, low-frequency Raman spectroscopy, WAXD, two-dimensional correlation spectroscopy, homospectral 2D-COS, heterospectral 2D-COS, intermolecular hydrogen bond

(Received November 13, 2019; Accepted December 17, 2019; Advance Publication Released Online by J-STAGE December 27, 2019)

Introduction

The massive production of petro-based plastic materials has accelerated the depletion of limited petroleum supplies and caused serious damage to our environment. Plastic waste accumulated in landfills will inhibit the circulation of liquids and gases, and delay the stabilization of organic matter.[1-3] Various disposal methods have been constantly introduced to promote environmental awareness, yet only a few of them show significant results. Therefore, the development of biodegradable polymers as an attempt to replace fossil-based plastic materials has received keen interest from the perspective of environmental protection.[4,5]

Poly(3-hydroxybutyrate) (PHB) is the most well-known biodegradable polymer synthesized from various gram-positive and -negative bacteria.[6,7] PHB is a member of the aliphatic polyesters, which are in high demand for commercial-scale production due to their thermoplastic properties.[8,9] PHB also shows unfavorable properties that include a high melting point (T_m) and high glass transition temperature (T_g), which need to be eliminated.[9] Modifications of PHB by copolymerization[10-12] and blending[13-18] processes with various synthetic and natural polymers have been intensively studied to improve the PHB physical properties.

Polymer blending is the simplest and less costly method for modifying the physical properties of a polymer. PHB was found to be miscible with poly(4-vinylphenol) (PVPh) in the whole blending ratio.[15] PHB/PVPh blends were characterized from a previous differential scanning calorimetry (DSC) study; the blends in all blending ratios showed one-glass transition temperature (T_g) and negative numbers of the equilibrium melting point.[15] The miscibility of PHB/PVPh was mainly governed by a specific intermolecular hydrogen bond between each molecule, which can promote compatibility and miscibility, and has meaningful effects on the properties of the blends.[16-18] Previous investigations using Fourier-transform infrared spectroscopy (FTIR) and wide-angle X-ray diffraction (WAXD)

† To whom correspondence should be addressed.
E-mail: hsato@tiger.kobe-u.ac.jp (H. S.); ymjung@kangwon.ac.kr (Y. M. J.)

of PHB/PVPh revealed the existence of the strong intermolecular C=O···H–O hydrogen bond between PHB and PVPh.[16]

The spectroscopic studies of PHB and PHB modified polymers have been expanded from infrared (IR)[16,17,19-21] and Raman[12] spectroscopies to terahertz (THz)[10,18,22-24] spectroscopy in order to further study the inter and intramolecular hydrogen bonds. The THz frequency region is the region of about 3.3 – 333 cm^{-1}, and a THz spectrum of a polymer contains information about both intramolecular and intermolecular vibrational motions from the molecule.[25] Therefore, THz spectroscopy is an effective tool for investigating the higher-order structure and noncovalent bonds among a polymer chain, which are keys to understanding the properties of the polymer. In our latest THz study, we reported the existence of a weak band at 135 cm^{-1} in far-infrared (far-IR) spectra of PHB/PVPh blends, which is due to the intermolecular C=O···H–O hydrogen bond.[18]

Nevertheless, polymer structures are so complex to be analyzed using only a standard spectroscopic analysis method that a powerful spectral analytical technique, two-dimensional correlation spectroscopy (2D-COS), may be useful for investigating the polymer system.[26] 2D-COS has been applied in various fields of spectroscopies for comprehensive assessment of spectral data obtained under the influence of a perturbation, such as time, mechanical, electrical, thermal, and chemical.[27] 2D-COS can give new insights into understanding a system, such as establishment of band assignments, interpretation of spectral correlation, and determination of sequential order of intensity variations of bands. It has also several important benefits to massively improve spectral resolution and to investigate inter or intramolecular interactions.[28,29] 2D-COS analysis of THz spectral variation of PHB during the isothermal crystallization process has been carried out by Hoshina *et al.*[30,31] In that study, the researchers were able to separate the overlapping vibrational bands and reveal the sequential order in the isothermal crystallization process.[30,31]

This study is the advanced analysis of far-IR, low-frequency Raman, and WAXD results by homospectral and heterospectral 2D-COS, and is intended to deepen our understanding of the origin and existence of the PHB/PVPh intermolecular hydrogen bond. Reportedly, this may be the first study of heterospectral 2D-COS aimed at determining the correlation between far-IR and low-frequency Raman spectra.

Experimental

Materials and sample preparation

Biodegradable PHB (M_n = 65000) and PVPh (M_n = 11000) were obtained from Aldrich Japan Co. The solvents of chloroform and 2-butanone were supplied by Junsei Chemical Co. Ltd. and FUJIFILM Wako Pure Chemical Corporation, respectively. The samples investigated in this study were the same as those reported in Ref. 18. Several blending ratios of PHB/PVPh were prepared by solution-casting method without any purification process. Solutions of PHB in chloroform and PVPh in 2-butanone were mixed homogenously in several blending ratios then cast in petri dishes followed by evaporation at 27°C to obtained mass samples. Film samples for measurement were then prepared with a thickness of approximately 100 μm for measurements by hot-press method; the mass samples were heated and pressed at their melting temperature. To enhance the crystallization, the obtained film samples were kept in a vacuum-dried oven at 60°C for 12 h.

Far-IR, low-frequency Raman, and WAXD measurements

The far-IR, low-frequency Raman, and WAXD measurements in this study were performed as in the previous study.[18] Far-IR spectra of PHB/PVPh were measured by using a FARIS (JASCO Co.). For this spectrometer, a high-pressure mercury lamp was equipped as a light source, a Mylar™ film as a beam splitter, and superconducting bolometer (QMC: QNbB/PTC) as a detector. Far-IR spectra were obtained in the region of 300 – 50 cm^{-1} with scan number of 100 and a wavenumber resolution of 2 cm^{-1}. Water vapor inside the sample compartment was eliminated by purging nitrogen gas before measurement.

Low-frequency Raman spectra were measured by a Terahertz-Raman system SureBlock™ XLF-CLM from ONDAX. The instrument was connected with a HyperFlux U1 spectrometer by Tornado and a Mity CCD H10141 detector. The excitation wavelength of this low-frequency Raman system was 830 nm, and the wavenumber resolution was 3.5 cm^{-1}. The PHB/PVPh low-frequency Raman spectra were recorded in the 1500 – 50 cm^{-1} region with an exposure time of 0.2 s and scan number of 300.

WAXD studies were performed by using a BL03XU beamline at SPring-8, Harima, Japan. The wavelength of the incident beam was 1.0 Å, and the sample-to-detector distance for measurement was set to 77 mm. Two-dimensional WAXD patterns were recorded using a silicon-on-insulator photon imaging array sensor (SOPHIAS) detector with exposure time of 1 s.

Generating 2D-COS

The obtained far-IR, low-frequency Raman, and WAXD data were pre-processed using the following methods before 2D-COS analysis for each set of the spectra. The far-IR spectra were baseline corrected and area normalized using PLS_Toolbox 8.1 software (Eigenvector Research, Inc., Wenatchee, WA, USA) for MATLAB R2018b (The Mathworks Inc., Natick, MA, USA). The low-frequency Raman spectra were offset and normalized. The WAXD patterns were baseline corrected. Synchronous and asynchronous 2D correlation spectra of far-IR spectra, low-frequency Raman spectra, and WAXD pattern were obtained using MATLAB. The red and blue lines represent positive and negative cross peaks, respectively.

Results and Discussion

Figures 1(a) and 1(b) show chemical structures of PHB and PVPh, respectively. Schematic illustrations of intermolecular hydrogen bonds (HB)s in PHB, PHB/PVPh blends, and on pure PVPh are presented in Figs. 1(c) – 1(f). The lamellar crystal structure of PHB has a weak intermolecular C=O···H–C HB between a C=O group of one PHB chain and one of the C–H groups in a CH_3 side group of another chain (Fig. 1(c)).[19,20] PHB/PVPh blends are known to have an intermolecular C=O···H–O HB between a PHB helical structure and PVPh amorphous structure (Fig. 1(d)).[16,17] The amorphous structure of PVPh has two kinds of hydrogen bonds; self-associated HB between the OH groups (Fig. 1(e)) and π-associated HB between the C_6H_5 groups and OH groups (Fig. 1(f)).[16,17]

2D-COS of far-IR spectra

Figure 2 shows far-IR spectra of PHB/PVPh with various blend ratios (30/70), (40/60), (50/50), (60/40), (70/30), (80/20), (90/10), and (100/0). Five major bands can be observed at 264, 221, 179, 96, and 83 cm^{-1} due to PHB-crystalline phase. In the case of PHB/PVPh (0/100), (10/90), and (20/80), no band can

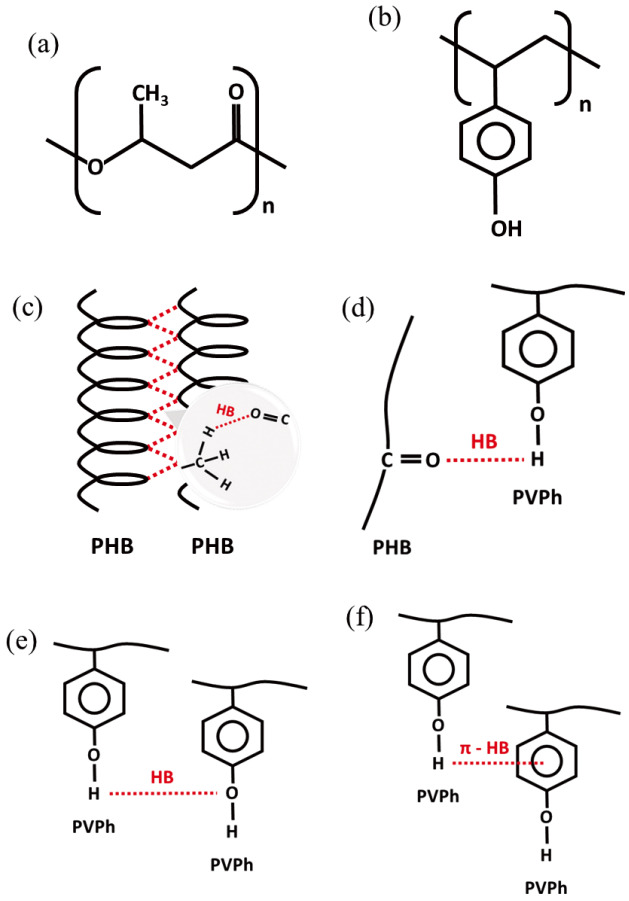

Fig. 1 Chemical structures of (a) poly(3-hydroxybutyrate) (PHB) and (b) poly(4-vinylphenol) (PVPh) and schematic illustration of intermolecular hydrogen bonds (HB)s: (c) C=O···H–C between PHB-PHB, (d) C=O···H–O between PHB-PVPh, (e) O–H···O–H between PVPh-PVPh, and (f) π···O-H between PVPh-PVPh.

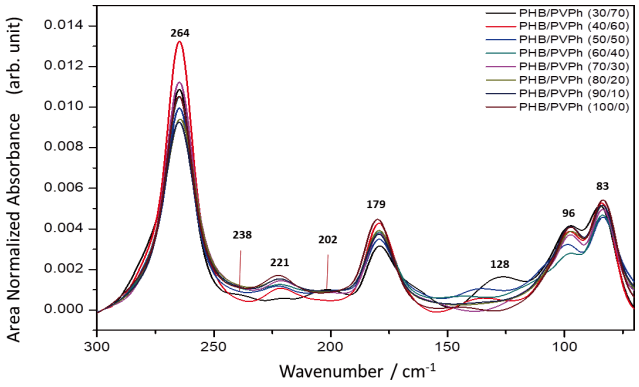

Fig. 2 Blend ratio-dependent far-IR spectra of PHB/PVPh; (30/70), (40/60), (50/50), (60/40), (70/30), (80/20), (90/20), and (100/0).

be observed due to their amorphous phase.[18] Band assignments described in Table 1 have been performed based on the quantum chemical calculation with Cartesian coordinate tensor transfer (CCT) method reported by Yamamoto *et al.*[32] The band at 264 cm^{-1} was assigned to the atomic motion of OCH (along *a* axis) + CH_3. The band at 179 cm^{-1} was ascribed to the motion of CH_2 + CH_3, the one at 96 cm^{-1} was due to the motion of

Table 1 Assignment of far-IR and low-frequency Raman bands[32]

Far-IR/cm^{-1}	Low-frequency Raman/cm^{-1}	Assignment
264		OCH (along *a* axis) + CH_3
221		
179		CH_2 + CH_3
	107	
96	98	COO + CH_2 + CH_3
83	79	C=O (o.p.) + CH_3
		COO + CH_2 + CH_3

COO + CH_2 + CH_3, and the one at 83 cm^{-1} was assigned to the mode of out of-plane C=O + CH_3 coupled with the mode of COO + CH_2 + CH_3.[32] There was difficulty in the assignment of the band at 221 cm^{-1} due to residual mismatch in the calculation process.[32] The polarization directions of the bands at 96 and 83 cm^{-1} explored in the same study more clearly revealed that they reflected the spring-like motion of the helical structure and the intermolecular interaction among PHB chains, respectively.[32]

Weaker bands at 238, 202, and 128 cm^{-1} have also been observed, as shown in Fig. 2. Those bands appeared clearly at PHB/PVPh (30/70) due to the PVPh amorphous phase. It indicates that in this blending ratio, PHB/PVPh shows the lowest crystalline feature as has been mentioned in the previous study.[18] The position of the band at 128 cm^{-1} shifts to the higher wavenumber by increasing PHB content. It implies that this band is sensitive to structural transformation due to changes in the blending ratio. It has been identified that pure PHB has the C=O···H–C intermolecular hydrogen bond between two helical chains of PHB crystalline structure, while PHB/PVPh less-order crystalline structures of the blends of (30/70), (40/60), (50/50), and (60/40) form the C=O···H–O intermolecular hydrogen bond between PHB and PVPh molecules.[16-18]

To better understand the effect of PHB content on the PVPh, 2D-COS was applied to the far-IR spectra of PHB/PVPh blend. Synchronous and asynchronous 2D correlation spectra for the blend ratio-dependent far-IR spectra of PHB/PVPh are shown in Fig. 3. There are seven autopeaks at 278, 264, 222, 181, 161, 128, and 96 cm^{-1} in the power spectrum displayed on the top of the synchronous 2D correlation spectrum, which is extracted along the diagonal line of the synchronous 2D correlation spectrum. There are negative cross peaks at (222, 264) and (161, 264) cm^{-1}, and a positive cross peak at (128, 264) cm^{-1}. It indicates that the presence of PVPh to PHB has a meaningful effect on the band at 264 cm^{-1}, and the 128 cm^{-1} band may correspond to the PVPh components.

The peak at 264 cm^{-1} shown in the synchronous 2D correlation spectrum is resolved into two peaks at 264 and 258 cm^{-1} in the asynchronous 2D correlation spectrum, which are ascribed to the PHB crystalline phase and bandwidth variation of the far-IR spectra due to blend-ratio change, respectively.[33] The peak at 128 cm^{-1} in the synchronous spectrum split into three peaks at 148, 138, and 127 cm^{-1} in the asynchronous spectrum, which associate with the shift of the band at 128 cm^{-1} in the far-IR spectra. From the sign of cross peaks in the synchronous and asynchronous 2D spectra, we can determine the sequential order of the intensity changes of bands with increasing PHB content as follows;

128 cm^{-1} (intermolecular HB PHB-PVPh)↓ ⟶ 96 cm^{-1} (PHB helix)↑ ⟶ 83 cm^{-1} (intermolecular HB PHB-PHB)↑ ⟶ 264 cm^{-1} (high-order PHB)↑

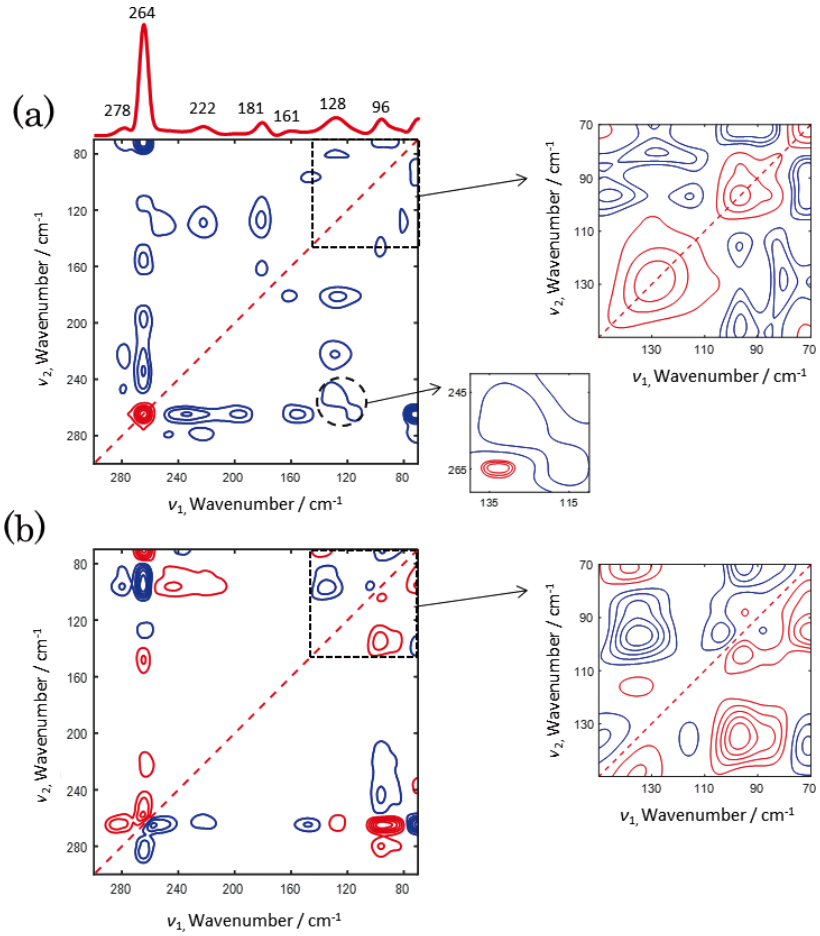

Fig. 3 (a) Synchronous and (b) asynchronous 2D correlation spectra of blend ratio-dependent far-IR spectra of PHB/PVPh (30/70), (40/60), (50/50), (60/40), (70/30), (80/20), (90/20), and (100/0). Inserted are the enlarged synchronous and asynchronous 2D correlation spectra in the 150 – 70 cm^{-1} region (black square) and in the hetero-region of 140 – 110 and 270 – 240 cm^{-1} (black circle).

By increasing PHB content in the PHB/PVPh blends, the amorphous structure of the blend gradually changes to the less-order structure and finally to the high-order structure following a certain process. This process starts with the reduction of the C=O···H–O hydrogen bond between PHB-PVPh, the growth of small PHB crystal nucleus in the system, the formation of the C=O···H–C hydrogen bond between PHB-PHB, and finally the development of the high-order crystalline structure. Sugawara *et al.* reported the sequential order of unimodal waveform in generalized 2D-COS.[34] However, we focus on the sequential order of the intensity maximum positions along the perturbation axis in our research.

2D-COS of low-frequency Raman spectra

Figure 4 shows the blend ratio-dependent low-frequency Raman spectra of PHB/PVPh. In the region of about 150 – 70 cm^{-1}, the neat PVPh shows only one broad band at around 79 cm^{-1} arising from its amorphous form. On the other hand, a sharp band at 79 cm^{-1} and two shoulder bands at around 107 and 98 cm^{-1} can be observed for PHB 100%. The band at 98 cm^{-1} directly reflects the spring-like motion of the helical structure, and the band at 79 cm^{-1} is assigned the intermolecular C=O···H–C hydrogen bond between two PHB helical chains.[32] Table 1 summarizes the band assignments.

Figure 5 displays 2D correlation spectra of blend ratio-dependent low-frequency Raman spectra of PHB/PVPh; (30/70), (40/60), (50/50), (60/40), (70/30), (80/20), (90/10), and (100/0). There are three auto-peaks at 111, 99, and 81 cm^{-1} extracted from the 2D correlation synchronous spectrum. Two cross peaks at (99, 81) and (111, 81) cm^{-1} show positive signs, indicating that the spectral intensity changes of all bands occur in the same direction. In the asynchronous 2D spectrum,

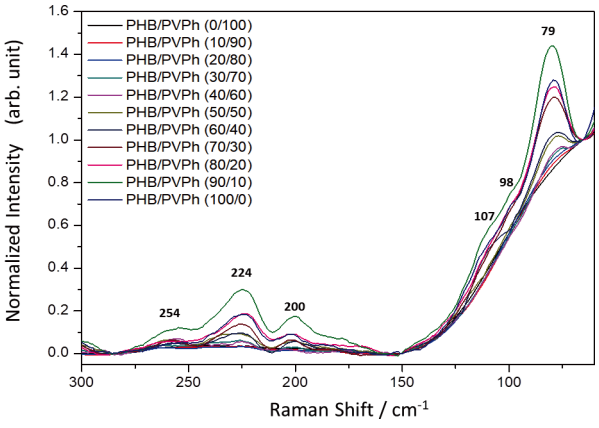

Fig. 4 Blend ratio-dependent low-frequency Raman spectra of PHB/PVPh.

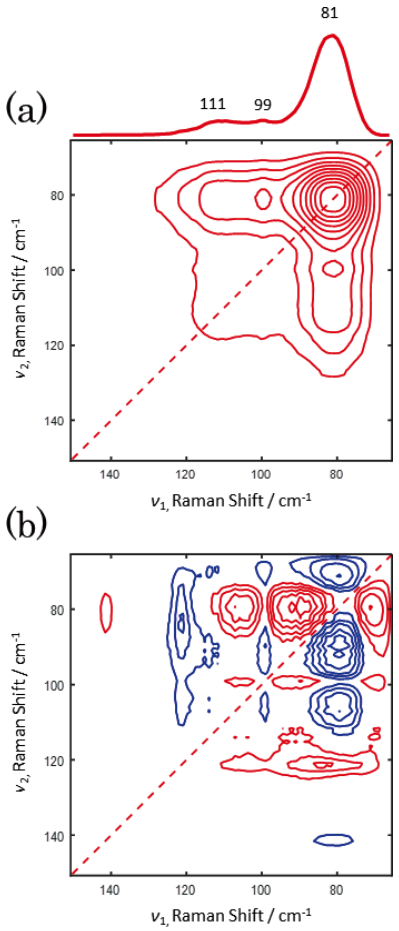

Fig. 5 (a) Synchronous and (b) asynchronous 2D correlation spectra of blend ratio-dependent low-frequency Raman spectra of PHB/PVPh; (30/70), (40/60), (50/50), (60/40), (70/30), (80/20), (90/20), and (100/0).

six peaks appear at 71, 79, 89, 99, 107, and 120 cm^{-1}. From the analysis of 2D correlation spectra, the sequential order of the intensity changes of the bands with increasing the PHB content can be determined as follows;

71 cm^{-1} (PVPh) ⟶ 99 cm^{-1} (PHB helix) ⟶
79 cm^{-1} (intermolecular HB PHB-PHB)

It indicates the same process as that for 2D correlation spectra of far-IR. By increasing PHB content in the PHB/PVPh blends, a small PHB crystal nucleus appears first, followed by the formation of the C=O···H-C hydrogen bond, and finally high-order crystalline structure develops.

2D-COS of WAXD patterns

Figure 6 depicts the blend ratio-dependent WAXD patterns of PHB/PVPh. There is no WAXD profile for the 100% PVPh due to its amorphous state. Two major peaks at 8.78 and 10.98° and a small broad peak at 10.57° arise from the PHB crystalline state, reflecting the diffractions from the (020), (110), and (011) PHB crystalline planes, respectively.[18,35] 2D correlation WAXD patterns of PHB/PVPh (30/70), (40/60), (50/50), (60/40), (70/30), (80/20), (90/10) and (100/0) are shown in Fig. 7. There are two peaks at 8.80 and 11.03° in the power spectrum of the synchronous 2D correlation spectrum. In the asynchronous spectrum, these two peaks at 8.80 and 11.03° are each resolved into two peaks at (8.87 and 8.78°) and (11.11 and 10.98°),

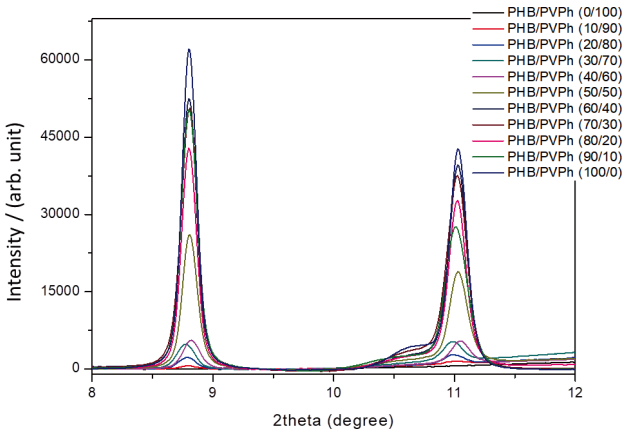

Fig. 6 Blend ratio-dependent WAXD patterns of PHB/PVPh.

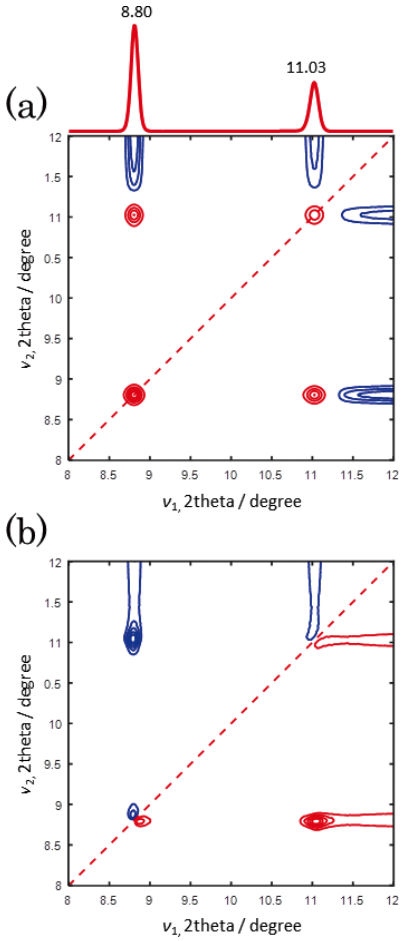

Fig. 7 (a) Synchronous and (b) asynchronous 2D correlation spectra of blend ratio-dependent WAXD patterns of PHB/PVPh; (30/70), (40/60), (50/50), (60/40), (70/30), (80/20), (90/20), and (100/0).

respectively. 2D correlation spectra of WAXD patterns indicate that the structure of the PHB/PVPh blend changes from a less-order crystalline structure to a high-order crystalline structure by increasing PHB content.

2D hetero correlation spectra

Figures 8(a), 8(b), and 8(c) show synchronous 2D heterospectral far-IR/low-frequency Raman, far-IR/WAXD, and low-frequency

Raman/WAXD correlation spectra of PHB/PVPh (30/70), (40/60), (50/50), (60/40), (70/30), (80/20), (90/10) and (100/0), respectively. The 2D heterospectral correlation analysis provides very important results that are hardly detected in the conventional 2D correlation analysis. 2D heterospectral correlation analysis both between closely related spectroscopic measurements and between completely different types of spectroscopic or physical techniques provide very attractive and rich insights for better understanding its complementary vibration spectra.[29] The 2D heterospectral correlation analysis has become one of the most active areas of research in 2D correlation spectroscopy. A positive cross peak in the synchronous 2D heterospectral correlation spectrum means that the two peaks (far-IR and low-frequency Raman, far-IR and WAXD, or low-frequency Raman and WAXD in this study) sharing a cross peak have the same origin, while a negative cross peak means that the two peaks have different origins.

In the synchronous 2D heterospectral far-IR/low-frequency Raman correlation spectrum (Fig. 8(a)), a far-IR peak at 130 cm^{-1} is negatively correlated with three low-frequency Raman peaks at 81, 100, and 110 cm^{-1}, while a far-IR peak at 96 cm^{-1} is positively correlated with low-frequency Raman peaks at 81 and 100 cm^{-1}. The 2D heterospectral results reveal that the peaks at 96 cm^{-1} in far-IR and those at 81, 100, and 110 cm^{-1} in the low-frequency Raman have the same origin, while the peaks at 130 cm^{-1} in the far-IR and those at 81, 100 and 110 cm^{-1} in the low-frequency Raman have different origins. The heterospectral correlation analysis also provides good evidence for the existence of the weak peaks at 100 and 110 cm^{-1}. In the synchronous 2D heterospectral far-IR/WAXD correlation spectrum (Fig. 8(b)), three far-IR peaks at 130, 102, and 90 cm^{-1} are negatively correlated with two WAXD peaks at 8.78 and 11.01°. In the synchronous 2D heterospectral low-frequency Raman/WAXD correlation spectrum (Fig. 8(c)), two low-frequency Raman bands at 109 and 80 cm^{-1} are positively correlated with two WAXD peaks at 8.76 and 10.98°.

The new peak observed at around 130 cm^{-1} in the far-IR spectra showed negative correlations with the peaks in the low-frequency Raman spectra at 81, 100, and 110 cm^{-1}; and WAXD profile at 8.78 and 11.01°. It indicated that those far-IR, low-frequency Raman, and WAXD peaks have different origins. The far-IR peak at 130 cm^{-1} refers to the intermolecular C=O···H–O hydrogen bond between PHB and PVPh. Those peaks for low-frequency Raman and WAXD are attributed to the PHB crystalline bands. These results strengthen the conclusion of our previous study on PHB/PVPh intermolecular interaction by far-IR spectroscopy.[18]

The 2D-heterocorrelation of far-IR and low-frequency Raman spectra and WAXD patterns in this study gave new insight and valuable information. The weak peak due to the intermolecular hydrogen bond between PHB and PVPh in the amorphous phase was detected clearly. In addition, it was found that its origin was not from the crystal structure.

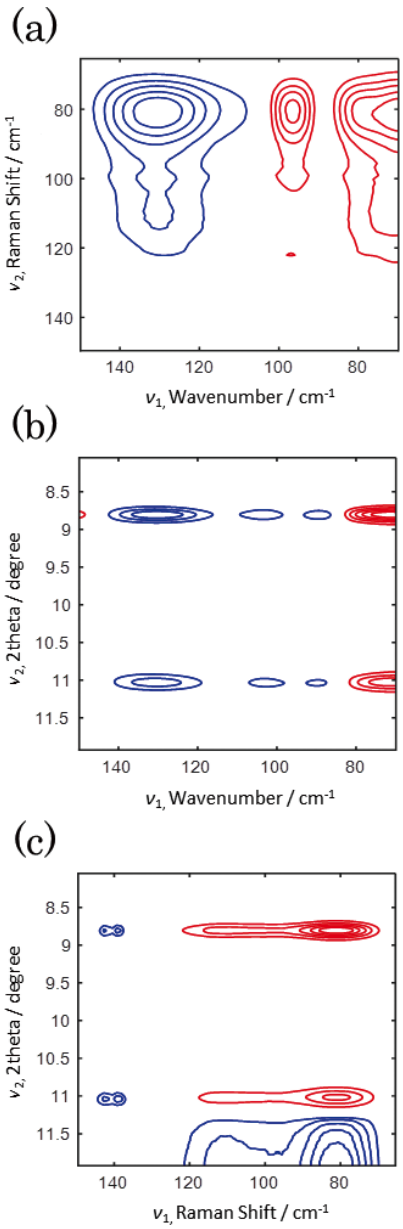

Fig. 8 Synchronous 2D heterospectral correlation of blend ratio-dependent (a) far-IR/low-frequency Raman (b) far-IR/WAXD and (c) low-frequency Raman/WAXD of PHB/PVPh; (30/70), (40/60), (50/50), (60/40), (70/30), (80/20), (90/20), and (100/0).

Conclusions

Homospectral and heterospectral 2D-COS analysis of far-IR, low-frequency Raman, and WAXD profile as a function of the blend ratio of PHB/PVPh have been performed in this study. New interesting information was obtained from the 2D-COS results. The 2D-COS of the far-IR spectra with various blend ratios revealed that two far-IR peaks at 264 and 128 cm^{-1} correspond to PVPh components. Moreover, it was found that these two peaks are the overlapped peaks at 264 and 258 cm^{-1} for the former; those at 148, 138, and 127 cm^{-1} for the latter, even they look like an ordinary band. The 2D-COS results of the low-frequency Raman spectra of PHB/PVPh with various blend ratios are in good agreement with those for far-IR spectra. The 2D-COS WAXD patterns of PHB/PVPh revealed that peaks at 8.80 and 11.03° come from two overlapped peaks at (8.87 and 8.78°) and (11.11 and 10.98°), respectively. Synchronous 2D heterospectral of far-IR/low-frequency Raman, far-IR/WAXD, and low-frequency Raman/WAXD correlation spectra of PHB/PVPh have also been investigated. The result indicated that the new peak observed at around 130 cm^{-1} in the far-IR spectra refers to the intermolecular C=O···H–O hydrogen bond between PHB and PVPh. While, the peaks for low-frequency Raman at 81, 100, and 110 cm^{-1} and WAXD profiles at 8.78 and 11.01° are attributed to the PHB crystalline bands. This has been concluded from the negative correlation of all of the bands.

References

1. C. J. Rhodes, *Sci. Prog.*, **2018**, *101*, 207.
2. D. Lithner, Å. Larsson, and G. Dave, *Sci. Total Environ.*, **2011**, *409*, 3309.
3. E. L. Teuten, J. M. Saquing, D. R. U. Knappe, M. A. Barlaz, S. Jonsson, A. Björn, S. J. Rowland, R. C. Tompson, T. S. Galloway, R. Yamashita, D. Ochi, Y. Watanuki, C. Moore, P. H. Viet, T. S. Tana, M. Prudente, R. Boonyatumanond, M. P. Zakaria, K. Akkhavong, Y. Ogata, H. Hirai, S. Iwasa, K. Mizukawa, Y. Hagino, A. Imamura, M. Saha, and H. Takada, *Phil. Trans. R. Soc. B*, **2009**, 3*64*, 2027.
4. R. C. Thompson, C. J. Moore, F. S. vom Saal, and S. H. Swan, *Phil. Trans. R. Soc. B*, **2009**, *364*, 2153.
5. M. Rujnić-Sokele and A. Pilipović, *Waste Manag. Res.*, **2017**, *37*, 132.
6. M. Koller, A. Salerno, A. Muhr, A. Reiterer, and G. Braunegg, *Mater. Technol.*, **2013**, *47*, 5.
7. D. Y. Kim, H. W. Kim, M. G. Chung, and Y. H. Rhee, *J. Microbiol.*, **2007**, *45*, 87.
8. S. Philip, T. Keshavarz, and I. Roy, *J. Chem. Technol. Biotechnol.*, **2007**, *82*, 233.
9. Y. Dai, L. Lambert, Z. Yuan, and J. Keller, *J. Biotec.*, **2008**, *134*, 137.
10. D. Marlina, H. Sato, H. Hoshina, and Y. Ozaki, *Polymer*, **2018**, *135*, 331
11. X. J. Loh, Z. Zang, Y. Wu, and T. S. Lee, *Macromolecules*, **2009**, *42*, 194.
12. I. Noda, A. Roy, J. Carriere, B. J. Sobieski, D. B. Chase, and J. F. Rabolt, *Appl. Spectrosc.*, **2017**, *71*, 1427.
13. M. J. K. Chee, J. Ismail, C. Kummerlöwe, and H. W. Kammer, *Polymer*, **2002**, *43*, 1235.
14. I. Armentano, E. Fortunati, N. Burgos, F. Dominici, F. Luzi, S. Fiori, A. Jiménez, K. Yoon, J. Ahn, S. Kang, and J. M. Kenny, *Express Polym. Lett.*, **2015**, *9*, 583.
15. P. Xing, L. Dong, Y. An, Z. Feng, M. Avella, and E. Mastuscelli, *Macromolecules*, **1997**, *30*, 2726.
16. L. Guo, H. Sato, T. Hashimoto, and Y. Ozaki, *Macromolecules*, **2010**, *43*, 3897.
17. L. Guo, H. Sato, T. Hashimoto, and Y. Ozaki, *Macromolecules*, **2011**, *44*, 2229.
18. D. Marlina, H. Hoshina, H. Sato, and Y. Ozaki, *Polymer*, **2019**, *181*, 121790.
19. H. Sato, R. Murakami, A. Padermshoke, F. Hirose, K. Senda, I. Noda, and Y. Ozaki, *Macromolecules*, **2004**, *37*, 7203.
20. H. Sato, K. Mori, R. Murakami, Y. Ando, I. Takahashi, J. Zhang, H. Terauchi, F. Hirose, K. Senda, K. Tashiro, I. Noda, and Y. Ozaki, *Macromolecules*, **2006**, *39*, 1525.
21. H. Sato, Y. Ando, H. Mitomo, and Y. Ozaki, *Macromolecules*, **2011**, *44*, 2829.
22. H. Hoshina, Y. Morisawa, H. Sato, A. Kamiya, I. Noda, Y. Ozaki, and C. Otani, *Appl. Phys. Lett.*, **2010**, *96*, 101904.
23. H. Hoshina, Y. Morisawa, H. Sato, H. Minamide, I. Noda, Y. Ozaki, and C. Otani, *Phys. Chem. Chem. Phys.*, **2011**, *13*, 9173.
24. H. Hoshina, S. Ishii, S. Yamamoto, Y. Morisawa, H. Sato, T. Uchiyama, Y. Ozaki, and C. Otani, *IEEE Trans. Terahertz Sci. Technol.*, **2013**, *3*, 248.
25. Y.-S. Lee, "*Principle of Terahertz Science and Technology*", **2009**, Springer, New York, USA.
26. Y. Park, S. Jin, Y. Park, S. M. Kim, I. Noda, B. Chae, and Y. M. Jung, *Polymers*, **2019**, *11*, 507.
27. Y. Park, I. Noda, and Y. M. Jung, *J. Mol. Struct.*, **2016**, *1124*, 11.
28. Y. Park, S. Jin, I. Noda, and Y. M. Jung, *J. Mol. Struct.*, **2018**, *1168*, 1.
29. Y. M. Jung and I. Noda, *Appl. Spectrosc. Rev.*, **2006**, *41*, 515.
30. H. Hoshina, S. Ishii, Y. Morisawa, H. Sato, I. Noda, Y. Ozaki, and C. Otani, *Appl. Phys. Lett.*, **2012**, *100*, 011907.
31. H. Hoshina, S. Ishii, and C. Otani, *J. Mol. Struct.*, **2014**, *1069*, 152.
32. S. Yamamoto, Y. Morisawa, H. Sato, H. Hoshina, and Y. Ozaki, *J. Phys. Chem. B*, **2013**, *117*, 2180.
33. M. A. Czarnecki, *Appl. Spectrosc.*, **2000**, *54*, 986.
34. T. Sugawara, T. Nakabayashi, and S. Morita, *Anal. Sci.*, **2018**, *34*, 845.
35. C. Wang, C. H. Hsu, and I. H. Hwang, *Polymer*, **2008**, *49*, 4188.